Shuai He, Ching-Tai Ng
A probabilistic approach for quantitative identification of multiple delaminations in laminated composite beams using guided waves
Engineering Structures, 2016; 127:602-614

A Probabilistic Approach for Quantitative Identification of Multiple Delaminations in Laminated Composite Beams Using Guided Waves

Shuai He and Ching-Tai Ng*

School of Civil, Environmental & Mining Engineering, The University of Adelaide, Adelaide, SA 5005, Australia

Abstract

In this study a probabilistic approach is proposed to identify multiple delaminations in laminated composite beams using guided waves. The proposed method is a model-based approach, which provides a quantitative identification of the delaminations. This study puts forward a practical damage identification method, and hence, it can identify multiple delaminations using guided wave signal measured at a single measurement point on the laminated composite beams. The proposed method first determines the number of delaminations using Bayesian model class selection method. The Bayesian statistical framework is then employed to not only identify the delamination locations, lengths and through-thickness locations, but also quantify the associated uncertainties, which provides valuable information for engineers in making decision on necessary remedial work. In addition the proposed method employs the time-domain spectral finite element method and Bayesian updating with Subset simulation to further improve the computational efficiency. The proposed probabilistic approach is verified and demonstrated using data obtained from numerical simulations, which consider both measurement noise and modeling error, and experimental data. The results show that the proposed method can accurately determine the number of

*Corresponding Author: Ching-Tai Ng (Email: alex.ng@adelaide.edu.au)

delaminations, and the identified delamination locations, lengths and through-thickness locations are closed to the true values.

Keywords: Multiple delaminations; Damage identification; Bayesian statistical framework; Bayesian model class selection; Guided waves; Spectral finite element; Subset simulation; Experiment

1 Introduction

1.1 Composite and non-destructive evaluation techniques

Laminated composite materials have been extensively used in many engineering applications, such as aerospace, mechanical and automotive engineering, due to their high strength, anti-corrosion and lightweight characteristics. Common defects occur in the laminated composite materials are fibre breaking, matrix cracking and delamination [1]. In particular the delamination could cause significant reduction in the stiffness and strength of structures and leads to structural failure. Detecting and identifying the delamination before structural failure are essential in improving the safety, durability and serviceability of the structures made by laminated composite materials.

Delamination is a separation of adjacent sub-surface laminae without any obvious visual evidence on the surface, and hence, non-destructive evaluation (NDE) techniques are required for detecting the delamination. Conventional NDE techniques, such as ultrasonic C-scan and A-scan, are point-to-point inspecting methods. They are time consuming and not able to inspect inaccessible locations of the structures. Low frequency vibration techniques [2] are efficient in inspecting large area of structures, however, they are insensitive to local defects, such as delamination.

1.2 Damage detection using guided waves

Guided wave has been widely recognized as one of the promising techniques for detecting the local defects [3, 4]. It is elastic stress wave, whose propagation characteristics depend on structural boundaries. Guided wave can be used to inspect large area of structural components due to its long propagation distances. Because guided waves are excited at high frequency, i.e. in the order of kilohertz, their wavelengths are small, and hence, they are sensitive to the local and incipient defects, e.g. delamination.

Recently, guided wave based damage detection techniques have been widely employed in identifying the defects in one-dimensional (1D), e.g. beams [5] and rods[6], and two-dimensional (2D) waveguides, e.g. plates [7-10] and shells [11]. For 2D waveguides, a number of damage detection techniques have been developed in the literature such as pre-stack reverse-time migration technique [12], tomography [13] and diffraction tomography [14, 15]. With the use of a transducer network, guided wave and scattered waves could be actuated and measured at different directions from the defect, respectively. This provides sufficient information for characterising the defects in 2D waveguides, e.g. defect location, size and shape. For 1D waveguides, most of the methods focused on determining the defect location based on the time-of-flight information of the reflected wave from the defect [16, 17]. There was relatively less work focused on the defect characterization, especially for delamination in the laminated composite beams.

Model-based approach has been employed to characterise the defects based on the measured guided wave signals in 1D waveguides. This approach treats defect parameters, such as defect location and size, as variables, by which the damage identification is achieved by minimising the discrepancy between the modelled and the measured guided wave signals. A number of model-based approaches have been

developed for characterising different types of defects, such as step damages [18-20] and cracks [21-23] in aluminium rods and beams. However, there were limited studies focused on delamination in laminated composite beams [24].

Recently the Bayesian statistical framework [25] has been applied to provide a quantitative identification of the defect in 1D waveguides [18] and this method was verified using experimentally measured guided wave signals [19]. It incooperated a spectral finite element (SFE) model in the Bayesian statitiscal framework to provide a computational efficient and quantatitive identification of the defect. One of the advantages of the Bayesian statistical framework is that it not only provides a characterization of the defect, i.e. identifying the defect location and size, but also quantifies the uncertainties associated with the defect identification results. This provides valuable information on making decision about the remedial work necessary to repair the strucutral damage.

1.3 Challenges in multiple delamination identification

In practical situation, the number of defects is unknown before the damage detection, and hence, the identification of multiple defects is a challenging issue for 1D waveguides, especially for a situation that the number of transducers is limited. For non-model based approach, it is difficult to determine the number of defects based on the information of the scattered waves as a number of scattered waves can be induced by multiple wave reflections between the defects. For multiple delaminations, the problem is more complicated. At each delamination region, the waveguide is divided into two individual sub-waveguides, and hence, reflection happens when the wave entering and leaving each of the delamination.

Although the model-based approach is able to provide quantitative identification of one defect, it has a difficulty in identifying multiple defects. In the situation that the

number of defects is unknown, the model considered more number of defects always has better fitting between the modeled and measured guided wave signals. Therefore, damage detection method based solely on the fitting between the modeled and the measured guided wave signals can be very misleading given the existence of modeling error and measurement noise in the measured data.

The aim of this study is to address the challenges in quantitative identification of multiple delaminations in laminated composite beams. The proposed method is developed based on the Bayesian statistical framework. The quantitative identification of the delaminations is achieved by solving a Bayesian updating problem, and hence, it could provide quantitative information of the delaminations, such as number of delaminations, delamination locations, lengths and through-thickness locations, and also the uncertainties associated with the damage identification results. To overcome the aforementioned challenge in identifying the multiple delaminations in laminated composite beams, the proposed method employs the Bayesian model class selection [26, 27] to provide a robust determination of the number of delaminations. In addition the proposed method employs the formulation of Bayesian updating with structural reliability method (BUS) [28], and hence, the Bayesian updating problem can be solved by a computational efficient and robust algorithm, i.e., Subset simulation [29-31]. In this study both numerical calculated and experimentally measured guided wave signals are used to verify and demonstrate the capability of the proposed method.

The paper is organised as follows. In Section 2 the details of the Bayesian approach for multiple delaminations identification are presented first. This section describes the Bayesian model class selection, Bayesian model updating, BUS formulation and Subset simulation for improving the computational efficiency and robustness of the proposed multiple delaminations identification method. Section 3 describes the SFE method and modelling of the delaminations. Section 4 presents the results of the numerical case

studies to verify the proposed multiple delaminations identification method. The numerical case studies consider different situations, such as different number of delaminations, delamination locations, lengths and through-thickness locations, to assess the performance of proposed method. Experimental verification is provided in Section 5 to demonstrate the practicability of the proposed method. Finally conclusions are drawn in Section 6.

2 Bayesian approach for multiple delaminations identification

The proposed Bayesian approach is developed based on the Bayesian model class selection and Bayesian model updating, which are used to determine the number of delaminations and provide quantitative identification of the delaminations. In the Bayesian approach, a laminated composite beam with length *L* and different number of delaminations are considered. A schematic diagram of the laminated composite beam with multiple delamination is shown in Figure 1. In this study we assume there are N_M delaminations existed in the laminated composite beam and they are represented by different model classes $\bar{\mathbf{M}} = \{M_j : j = 1, 2, ..., N_M\}$. M_j is the model class representing the laminated composite beam with j delaminations. The delamination parameters l_j and d_j are used to describe the location and length of *j*-th delamination. For the through-thickness location, k_j is used to describe the delamination located between the *k*-th and (*k*+1)-th layers of the laminated composite beam.

The selection of the 'optimal' model class solely based on the fitting between measured and simulated data is impractical. In order to address this problem, this study used the Bayesian model class selection method in selecting the "optimal" model class to identify the number of delaminations. In addition the delamination parameters and their associated uncertainties are identified by the Bayesian statistical framework. The following sub-sections describe the Bayesian model class selection, Bayesian model

updating, and BUS formulation with Subset simulation for identifying multiple delaminations in the laminated composite beam.

[Figure 1. Schematic diagram of the laminated composite beam with multiple delaminations]

2.1 Bayesian mode class selection for determining the number of delaminations

Consider a set of possible model classes $\bar{\mathbf{M}} = \{M_j : j = 1, 2, ..., N_M\}$, which represent laminated composite beams with j delaminations. Bayesian model class selection can be used to determine the probability of each model class conditional on a set of measured guided wave data *D* as [25, 26, 32]

$$P\left(M_j \middle| D, \bar{\mathbf{M}}\right) = \frac{p\left(D \middle| M_j\right) P\left(M_j \middle| \bar{\mathbf{M}}\right)}{p\left(D \middle| \bar{\mathbf{M}}\right)} \tag{1}$$

where $P\left(M_j \middle| \bar{\mathbf{M}}\right) = 1/\mathrm{N}_M$ is the prior probability of each model class M_j. $p\left(D \middle| \bar{\mathbf{M}}\right)$ is a normalising constant and $p\left(D \middle| M_j\right)$ is the evidence of the model class M_j that has the following expression

$$p\left(D \middle| M_j\right) = \int p\left(D \middle| \boldsymbol{\theta}_j, M_j\right) p\left(\boldsymbol{\theta}_j \middle| M_j\right) d\boldsymbol{\theta}_j \tag{2}$$

where $\boldsymbol{\theta}_j$ is a vector that consists of the uncertain delamination parameters, such as delamination locations l_j, lengths d_j and through-thickness locations k_j. $p\left(D \middle| \boldsymbol{\theta}_j, M_j\right)$ is the likelihood function, a larger value of which means there is a better fitting between the simulated and experimentally measured guided wave signals. However, direct numerical integration of Equation (2) is impractical because it involves a multi-dimensional integral [33]. Asymptotic approach can be used for calculating Equation (2) but they are only applicable to globally identifiable situation [26]. In order to evaluate the model evidence, this study employs an improved BUS formulation [29], and hence, the Bayesian updating with Subset Simulation can be used to efficiently

calculate the evidence of the model class. The details of the BUS formulation and Subset simulation will be described in the sub-section 2.3.

A challenging issue in the identifying multiple delaminations is that the model class with more delamination parameters can have better fitting between the simulated and the experimentally measured data as the extra delamination parameters tend to fit the measurement noise and modelling error. However, the Bayesian model class selection algorithm addresses this issue by automatically penalising more 'complex' model class, i.e. the model classes with more delaminations. This can be illustrated by considering the evidence from an information-theoretic point of view. Consider the logarithmic form of Equation (2) [25, 32, 34] as

$$\begin{aligned} \ln p\left(D\middle|M_j\right) &= \int \ln\left[\frac{p\left(D\middle|\boldsymbol{\theta}_j,M_j\right)p\left(\boldsymbol{\theta}_j\middle|M_j\right)}{p\left(\boldsymbol{\theta}_j\middle|D,M_j\right)}\right]p\left(\boldsymbol{\theta}_j\middle|D,M_j\right)d\boldsymbol{\theta}_j \\ &= \int \ln\left[p\left(D\middle|\boldsymbol{\theta}_j,M_j\right)\right]p\left(\boldsymbol{\theta}_j\middle|D,M_j\right)d\boldsymbol{\theta}_j - \int \ln\left[\frac{p\left(\boldsymbol{\theta}_j\middle|D,M_j\right)}{p\left(\boldsymbol{\theta}_j\middle|M_j\right)}\right]p\left(\boldsymbol{\theta}_j\middle|D,M_j\right)d\boldsymbol{\theta}_j \end{aligned} \tag{3}$$

where $\ln p\left(D\middle|M_j\right)$ is the log-evidence for the model class M_j. The log-evidence consists of the log-likelihood function and relative entropy between the prior and posterior distribution, which are the first and second term at the right side of Equation (3), respectively. The log-likelihood function is a data-fit term that indicates the plausibility of the model class M_j. The relative entropy between the prior and posterior distribution is a measure of the information gained about the complexity of the model class, and hence, it provides a penalty against more 'complex' model class. Therefore, the log-evidence value is able to provide a robust determination of the number of delaminations in the laminated composite beams.

2.2 Bayesian model updating for identifying the delamination parameters

For identifying the delamination parameters of a given model class M_j, i.e. the

delamination locations, lengths and through-thickness locations, the measured guided wave data D can be used to update the corresponding plausibility of the uncertain delamination parameters. The posterior probability density function (PDF) of the delamination parameters $\boldsymbol{\theta}_j$ is obtained as [33, 35]

$$p\left(\boldsymbol{\theta}_j \middle| D, M_j\right) \propto p\left(D \middle| \boldsymbol{\theta}_j, M_j\right) p\left(\boldsymbol{\theta}_j \middle| M_j\right) \tag{4}$$

where $p\left(\boldsymbol{\theta}_j \middle| M_j\right)$ is the prior PDF that reflects the initial engineering judgement of the delamination parameters. $p\left(D \middle| \boldsymbol{\theta}_j, M_j\right)$ is the likelihood function and is assumed following the Gaussian distribution with zero mean and standard deviation of the prediction error σ_j based on the Principle of Maximum information Entropy [25, 36, 37]

$$p\left(D \middle| \boldsymbol{\theta}_j, M_j\right) = \frac{1}{\left(2\pi\sigma^2\right)^{N_o N_t/2}} \exp\left(-\frac{1}{2\sigma_j^2} \mathrm{J}\ \left(t; \boldsymbol{\theta}_j\right) \right) \tag{5}$$

where N_o is the number of measurement points and $N_t = T/\Delta t$ is the number of time steps. T is the duration of measurement and Δt is the time steps. $\mathcal{J}\left(t; \boldsymbol{\theta}_j\right)$ is the goodness-of-fit function and is defined as

$$\mathcal{J}\left(t; \boldsymbol{\theta}_j\right) = \sum_{o=1}^{N_o} \sum_{t=1}^{N_t} \left[q_m\left(t\right) - q_s\left(t; \boldsymbol{\theta}_j\right) \right]^2 \tag{6}$$

where q_s is the simulation data and q_m is the experimentally measured data. In this study the simulation data is obtained from the SFE model described in Section 3. The variance σ^2 in the likelihood function is normally a positive real number and it is sampled randomly from the inverse of Gamma distribution $IG(0.5N_t N_o + 1, 0.5\mathcal{J}(t; \boldsymbol{\theta}_j))$ [38].

The BUS formulation with Subset simulation, which will be described in Section 2.3, is used in this study to draw samples from the target distribution, and hence, approximating the posterior PDF in Equation (4). Once the samples are asymptotically

distributed as $p\left(\boldsymbol{\theta}_j \mid D, M_j\right)$, the delamination parameters can be estimated by the sample means, where the sample c.o.v.s of the delamination parameters can be obtained by calculating the ratio of the sample standard deviation to the sample means. For determining the marginal posterior PDF of the each of the uncertain delamination parameters, the adaptive kernel density estimation with Gaussian distribution being the kernel PDF [39-41] can be used and it is defined as

$$k\left(\boldsymbol{\theta}_j(i)\right)=\frac{1}{N_s}\sum_{h=1}^{N_s}W^{(h)}\mathrm{N}\left(\boldsymbol{\theta}_j^{(h)}(i),\mathbf{C}(i,i)\right) \tag{7}$$

where $\mathrm{N}(\mu,\Sigma)$ is the multivariate Gaussian PDF with mean μ and covariance matrix Σ. $W^{(h)}$ is the weighting of the h^{th} sample and i is an index for choosing the uncertain delamination parameter in the marginal posterior PDF calculation. $\mathbf{C}(i,i)$ is the i^{th} diagonal element of the sample covariance matrix calculated by the samples when they are asymptotically distributed as $p\left(\boldsymbol{\theta}_j \mid D, M_j\right)$.

2.3 BUS formulation

This section describes the BUS formulation that allows the Bayesian updating problem to be solved by a computational efficient algorithm, Subset simulation. The BUS formulation converts the Bayesian problem to a reliability problem [28] with the purpose of determining the failure probability $P(F)$ of the failure event F. In the context of BUS, F can be defined as

$$F=\left\{cp\left(D\middle|\boldsymbol{\theta}_j,M_j\right)-U>0\right\} \tag{8}$$

where U is a random value between 0 and 1. c is a constant denoted the 'likelihood multiplier' satisfied the following inequality

$$cp\left(D\middle|\boldsymbol{\theta}_j,M_j\right)\le 1 \tag{9}$$

For any $c<c_{\max}$, the posterior samples $\boldsymbol{\theta}_j$ follows the posterior PDF $p\left(\boldsymbol{\theta}_j\middle|D,M_j\right)$

[29]. While the selected $c_{\max}$ for the multiplier significantly influences the efficiency and correctness of the sampling, its value is not available before the determination of the maximum likelihood value $p\left(D\middle|\hat{\boldsymbol{\theta}}_j,M_j\right)$ with the optimal parameter $\hat{\boldsymbol{\theta}}_j$. This is contradictory since $c_{\max}$ is required for seeking the correct optimal parameter $\hat{\boldsymbol{\theta}}_j$. In order to overcome this problem, the BUS formulation has recently been improved by Au, DiazDelaO and Yoshida [29], by which the failure event is transformed into the followed inequality

$$F=\left\{\ln\left[\frac{p\left(D\middle|\boldsymbol{\theta}_j,M_j\right)}{U}\right]>-\ln c\right\} \tag{10}$$

It can be rewritten as

$$F=\{Y>O\} \tag{11}$$

where $O=-\ln c$ and Y denotes the driving variable, which has the form

$$Y=\ln\left[\frac{p\left(D\middle|\boldsymbol{\theta}_j,M_j\right)}{U}\right] \tag{12}$$

Let O be an admissible threshold level, when O is larger than $O_{\min}=-\ln c_{\max}$ the posterior samples $\boldsymbol{\theta}_j$ will follow the posterior PDF $p\left(\boldsymbol{\theta}_j\middle|D,M_j\right)$. Consider the failure probability $P(F)$ can be estimated using the posterior samples from Subset simulation, $P(F)$ can be expressed by the evidence of the model class $p(D|M_j)$ [29]

$$P(F)=e^{-O}p\left(D\middle|M_j\right) \text{ for } O>O_{\min} \tag{13}$$

For sufficiently large *O*, Equation (13) shows that $P(F)$ will decay exponentially with O as $p(D|M_j)$ is constant for a given problem. $P(F)$ can be interpreted as the complementary cumulative distribution function (CCDF) of *Y*, where the exponential decay is similar to a typical CCDF in reliability analysis.

As shown in Equation (13), when $O>O_{\min}$ the failure probability $P(F)$ is

theoretically related to the evidence $p(D|M_j)$. However, $O_{\min}$ is not known in the actual implementation, therefore, it is essential to determine whether $O > O_{\min}$, and hence, the samples conditional on $\{Y > O\}$ are confidently collected as the correct posterior samples in the Subset simulation. In order to determine when the value of O has become larger than the unknown $O_{\min}$, the characteristic trends of the logarithmic failure probability in Equation (13) are investigated. Consider $\ln P(F) = -O + V(O)$, hence,

$$V(O) = \ln P(F) + O \tag{14}$$

At the beginning, $V(O)$ increases linearly with O as $\ln P(F) \approx 0$. This means $V(O)$ first increase linearly and then go through a transition until it settles at $V(O) = \ln p(D|M_j)$ when $O > O_{\min}$. Therefore, the log-evidence $\ln p(D|M_j)$ can be obtained as

$$\ln p(D|M_j) = O + \ln P(F) \text{ for } O > O_{\min} \tag{15}$$

2.4 Subset simulation for generating posterior samples

Based on the BUS formulation, the failure probability $P(F)$ can be evaluated using the posterior samples obtained from the conditional samples in the efficient Subset simulation [29]. Essentially, Subset simulation progressively generates conditional samples towards the target failure events through a series of intermediate failure events, which converts a rare reliability problem into a series of more frequent one. It is efficient and sustainable to the high dimension problem as the Markov Chain Monte Carlo (MCMC) sampling technique [33] is implemented in each intermediate step. As shown in Equation (15) once the failure probability $P(F)$ is evaluated and $O > O_{\min}$, the evidence $p(D|M_j)$ of the model class can be determined.

[Figure 2. Schematic framework of Subset simulation]

The schematic framework of Subset simulation is shown in Figure 2. In the Step 1 of the Subset simulation, the number of samples N for each stage and the probability level of the intermediate simulation P_0 need to be defined. It should be noted that NP_0 and $1/P_0$ are positive integrates. N i.i.d. (independent and identically distributed) samples are uniformly generated from the prior distribution using the standard Monte Carlo method and the corresponding driving variable Y is calculated using Equation (12).

In Step 2, Y is firstly rearranged in ascending order, giving an ordered list denoted by $\{O_r^{(s)} : r = 1,...,N\}$ for stage s. For $O_s < O_{\min}$, at which $O_s = O_{N(1-P_0)}^{(s)}$ is the $N(1-P_0)$-th sample in the ordered list, the last $P_0 N$ samples in the ordered list are used as 'seed' samples to simulate $P_0 N$ MCMC chains. These chains have equal sampling length as $1/P_0$, and hence, producing N new samples for the next Subset simulation level $s = s+1$. The failure probability at each stage *s* is obtained conditionally on the failure events from the previous stages as

$$P(F_r^{(s)}) = \prod_{f=0}^{s} P(F_r^{(s)} \mid F_r^{(s-1)}) = P_0^s \frac{N-r}{N} \quad \text{for} \quad r = 1,...,N \tag{16}$$

where $F_r^{(s)}$ is the failure event of stage *s*. From Equation (16) it is shown that the probability of the rare failure event can be gradually approximated in the Subset simulation. The failure probability $P(F_r^{(s)})$ is then used to evaluate the $O_{\min}$ as stated in the Section 2.3. Step 2 is repeated until $O_s > O_{\min}$.

Finally, in Step 3, the log-evidence of model class M_j is evaluated using Equations (15) and (16), and hence

$$\ln p(D \mid M_j) = O + \ln P(F) \approx O_s + s \ln P_0 \tag{17}$$

In the Bayesian approach the number of delamination and the delamination

parameters are assumed unknown initially. The approach first considers a model class with a delamination and identifies the delamination parameters by solving the Bayesian updating problem using the BUS formulation with Subset simulation. Once the delamination parameters are identified, the evidence of this model class is then evaluated. After that the Bayesian approach considers a more "complex" model class, e.g. two delaminations and repeated the aforementioned calculations. The procedure stops when the value of the evidence of the currently considered model class is smaller than the less "complex" model class. Therefore, the number of delaminations and the delamination parameters can be determined by the model class with the largest evidence value.

3 Time-domain spectral finite element method for modelling laminated composite beams with multiple delaminations

The modeling of guided wave propagation in laminated composite laminated using the SFE method is similar to the conventional FE method, in which the problem can be represented by the time-domain ordinary differential equation [42-44]

$$\mathbf{M}\ddot{\mathbf{U}}+\mathbf{C}\dot{\mathbf{U}}+\mathbf{K}\mathbf{U}=\mathbf{F}(t) \tag{18}$$

where $\mathbf{U}$, $\dot{\mathbf{U}}$ and $\ddot{\mathbf{U}}$ are the displacement, velocity and acceleration vector in time domain, respectively. $\mathbf{M}$ is the global mass matrix, $\mathbf{C}$ is the global damping matrix, $\mathbf{K}$ is the global stiffness matrix and $\mathbf{F}(t)$ is the global force vector at time *t*. The global mass matrix $\mathbf{M}$ and the stiffness matrix $\mathbf{K}$ are assembled using their element matrices [42, 43]. In this study the guided wave propagation in the laminated composite beam is simulated using the higher order theory along with the Poisson's contraction effect [45]. The displacement field in the composite beam can be written as

$$\bar{u}(x,y) \approx u(x) - \varphi(x) y \tag{19}$$

$$\bar{v}(x,y) \approx v(x) + \psi(x) y \tag{20}$$

where u and v are the axial and transverse displacements in the neutral axis of the beam as shown in Figure 3. φ is the rotation of the cross section and ψ is the contraction due to Poisson's effect. y is the vector of distance measured from the neutral axis. The strain field can be expressed as [45]

$$\varepsilon = \begin{bmatrix} \dfrac{\partial u}{\partial x} - y\dfrac{\partial \varphi}{\partial x} \\ \psi \\ \dfrac{\partial v}{\partial x} + y\dfrac{\partial \psi}{\partial x} - \varphi \end{bmatrix} \tag{21}$$

Based on the higher order theory along with the Poisson's contraction effect, the element mass matrix $\mathbf{M}^e$, element stiffness matrix $\mathbf{K}^e$ and the element force vector $\mathbf{F}^e(t)$ at time t used to formulated the corresponding global matrices in Equation (18) are

$$\mathbf{M}^e \approx \sum_{i=1}^{n} w_i \mathbf{N}_e(\xi_i)^T \mathbf{r} \mathbf{N}_e(\xi_i) \det\left(J(\xi_i)\right) \tag{22}$$

$$\mathbf{K}^e \approx b \sum_{i=1}^{n} w_i \sum_{k=1}^{N_k} \int_{h_{k-1}}^{h_k} \mathbf{B}_e(\xi_i)^T \bar{\mathbf{Q}}_k \mathbf{B}_e(\xi_i) \det\left(J(\xi_i)\right) dy \tag{23}$$

$$\mathbf{F}^e(t) \approx \sum_{i=1}^{n} w_i \mathbf{N}_e(\xi_i)^T \mathbf{f}_e(t) \mathbf{N}_e(\xi_i) \det\left(J(\xi_i)\right) \tag{24}$$

where b and N_k are the width and the total number of layer of the laminated composite beam. $J = \partial x / \partial \xi$ is the Jacobian function transferring the local coordinate to the global coordinate. h_k and h_{k-1} denote the height of upper and lower surface of the k-th layer, respectively. f_e is the external excitation. Different to the conventional FE method, the SFE method employs the Gauss-Lobatto-Legendre (GLL) nodes ξ_i in

each element. This leads to the diagonal form of the mass matrix that can be solved efficiently by the central difference scheme, and hence, reducing the mesh density. The local coordinate of the ξ_i can be determined by

$$\left(1-\xi_i^2\right)L'_{n-1}(\xi_i)=0 \quad \text{for} \quad \xi_i \in [-1,1] \quad \text{and} \quad i \in 1,...,n \tag{25}$$

where L'_{n-1} is the first derivative of the $(n\text{-}1)^{\text{th}}$ order Legendre polynomial. In this study n = 6. The distribution of the GLL nodes and their corresponding shape function value are shown in Figure 3. w_i is the weight of the corresponding GLL node ξ_i and is defined as

$$w_i = \frac{2}{n(n-1)[L_{n-1}(\xi_i)]^2} \tag{26}$$

where L_{n-1} is the $(n\text{-}1)^{\text{th}}$ order Legendre polynomial.

[Figure 3. Distribution of the 5^{th} *order GLL nodes and the corresponding shape function value of a spectral beam element]*

$\mathbf{B}_e$ is the strain-displacement operator and is defined as

$$\mathbf{B}^e = \begin{bmatrix} \dfrac{\partial}{\partial x} & -y\dfrac{\partial}{\partial x} & 0 & 0 \\ 0 & 0 & 0 & 1 \\ 0 & -1 & \dfrac{\partial}{\partial x} & y\dfrac{\partial}{\partial x} \end{bmatrix} \mathbf{N}^e \tag{27}$$

where $\partial/\partial x = J^{-1}\partial/\partial\xi$. $\mathbf{N}_e$ is the shape function matrix of the SFE element, which has the form

$$\mathbf{N}_e = \mathbf{N} \otimes \mathbf{I} \tag{28}$$

where $\mathbf{N} = [N_1(\xi),...,N_n(\xi)]$ is a row vector. $\mathbf{I}$ is a 4×4 identity matrix. '$\otimes$' is the Kronecker product. The shape function $N_i(\xi)$ at node i has the orthogonal property and can be calculated by

$$N_i(\xi) = \prod_{m=1, m\neq i}^{n} \frac{\xi - \xi_m}{\xi_i - \xi_m} \quad \text{for} \quad i(i \in 1,2,...,n) \tag{29}$$

where n is the number of GLL integration points in each element and m is the sequence of node. Using the shape function, the displacement fields are approximated as follow

$$\begin{bmatrix} u^e(\xi) \\ \varphi^e(\xi) \\ v^e(\xi) \\ \psi^e(\xi) \end{bmatrix} = \mathbf{N}^e\mathbf{q}^e = \sum_{i=1}^{n} \begin{bmatrix} N_i(\xi) & & & \\ & N_i(\xi) & & \\ & & N_i(\xi) & \\ & & & N_i(\xi) \end{bmatrix} \begin{bmatrix} q_u^e(\xi_i) \\ q_\varphi^e(\xi_i) \\ q_v^e(\xi_i) \\ q_\psi^e(\xi_i) \end{bmatrix} \tag{30}$$

where $\mathbf{q}^e$ is the vector of nodal displacement in the corresponding degrees-of-freedom. The matrix $\mathbf{r}$ from Equation (22) has the form

$$\mathbf{r} = \begin{bmatrix} I_0 & 0 & 0 & 0 \\ 0 & I_2 & 0 & 0 \\ 0 & 0 & I_0 & 0 \\ 0 & 0 & 0 & I_2 \end{bmatrix} \tag{31}$$

where

$$I_0 = b\sum_{k=1}^{N_k} \rho_k \left(h_k - h_{k-1}\right)$$

$$I_2 = b\sum_{k=1}^{N_k} \rho_k \left(h_k^3 - h_{k-1}^3\right)/3 \tag{32}$$

where ρ_k is the density of the k-th layer. In Equation (23), $\overline{\mathbf{Q}}_k$ is the material property matrix of the k^{th} layer of the laminated composite beam in the defined orientation and is defined as

$$\overline{\mathbf{Q}}_k = \begin{bmatrix} \overline{Q}_{11} & \overline{Q}_{13} & 0 \\ \overline{Q}_{13} & \overline{Q}_{33} & 0 \\ 0 & 0 & \overline{Q}_{55} \end{bmatrix} \tag{33}$$

where $\overline{Q}_{11}$, $\overline{Q}_{13}$, $\overline{Q}_{33}$ and $\overline{Q}_{55}$ can be found in [46]. In order to model the delamination, the intact beam elements e_1 and e_2, as shown in Figure 4, are separated into $e_{1\text{-up}}$, $e_{2\text{-up}}$ and $e_{1\text{-low}}$, $e_{2\text{-low}}$ elements to form a delamination element. Specifically,

the nodes in the intact beam elements are duplicated at the delaminated region and only the nodes at the delamination tips are connected. In this study the aforementioned SFE is used to model the laminated composite beam and the delamination element is used to model each of the delmainations. In addition the Hilbert transform [47] is first used to obtain the signal envelopes for the modeled and experimentally measured data guided wave signals. The signal envelopes are then used in the proposed Bayesian approach in Section 2 for identifying the number of delaminations, delamination locations, lengths and through-thickness locations.

[Figure 4. Modelling of the laminated composite beam with a delamination and zoom-in at the delamination]

4 Numerical case studies

A series of numerical case studies were used to systematically assess the performance of the proposed Bayesian multiple delaminations identification method with the consideration of different delamination scenarios. The numerical case studies considered a 500 mm long and 6 mm wide cross-ply laminated composite beam with stacking sequence of $[0/90/0/90]_s$. The total thickness of the beam is 2 mm, which consists of eight 0.25 mm thick unidirectional carbon/epoxy prepreg plies. The elastic properties of the each ply are shown in Table 1. In this study the fundamental anti-symmetric mode (A_0) guided wave was used as the incident wave as it has been demonstrated that it is sensitive to the delamination [48]. The excitation signal was an 80 kHz narrow-band five-cycle sinusoidal tone burst modulated by a Hanning window. The excitation was applied to the left end of the laminated composite beam and the guided wave signal was calculated at the same location. The duration of the calculated guided wave data in the numerical case studies allows the incident A_0 guided wave propagates from the excitation location to the beam end, and then reflects and

propagates back to the excitation location but the beam end reflected wave pulse was not included in the data.

The time-domain SFE method described in Section 3 was used to model the laminated composite beams with different numbers of delaminations and the models were treated as the identification model for simulating guided wave data q_s in Equation (6) of the proposed Bayesian approach. For each model class, the uncertainty delamination parameters are the locations l_j, lengths d_j and through-thickness locations k_j of the delaminations. In the time-domain SFE model, 12 mm long spectral elements with 8 GLL nodes were used to model the laminated composite beam. The time step Δt used in the simulation was $0.75e^{-7}$ sec to ensure the solution of the time-domain ordinary differential Equation (18) to be converged.

The laminated composite beams with delaminations were also modeled using the three-dimensional (3D) finite element method and the calculated data was treated as synthetic experimental data as q_m in Equation (6). Therefore the modeling error was considered in the numerical case studies as the synthetic experimental data was generated by 3D FE method. Commercial software ABAQUS v6.12-1 [49] was used to simulate the guided wave in this study. Eight-node 3D reduced integration solid brick element (C3D8R) was used and the mesh size was 0.3 mm. The A_0 guided wave was generated by applying shear traction at the edge of the left beam end. Enhanced hourglass control was enabled and the dynamic explicit solver was employed to solve the guided wave propagation. The time step in the simulation was automatically decided by ABAQUS. In this study the signal envelope calculated by the Hilbert transform [47] was used as the simulated data by SFE and synthetic experimental data by 3D FE to reduce the complexity of the signals. Measurement noise was considered in synthetic experimental data. It is assumed to be white noise and was taken to be 3% of the RMS of the noise-free signals.

[Table 1. Elastic properties of the the pre-preg lamina in the numerical case studies]

Five cases, i.e. Cases N1, N2, N3, N4 and N5, shown in Table 2 were used to study the performance of the proposed multiple delaminations identification method. For Cases N1, N2 and N3, one delamination was considered in the laminated composite beam and the length of delaminations (d_1) were 6 mm, 10 mm and 20 mm, respectively. They are all located at l_1 = 200 mm from the left beam end of the laminated composite beam. Case N4 considers two delaminations while Case N5 considers three delaminations. The Subset simulation was employed to generate the posterior samples, and hence, approximating the posterior PDF of the delamination parameters and probability of the model classes for each case. The assignment of the prior PDF for the location and length of the delamination are uniformly distributed over [10mm 490mm] and [1.3mm 18mm], respectively. The through-thickness location of the delamination is an integer and it has equal probability from k_j = 1 to 7. It should be noted that the delamination located at k_j = 1, 2 and 3 has the same effect for k_j = 7, 6 and 5, respectively, on the guided wave. The number of samples N at each stage of Subset simulation was set as 500 and the probability level of the intermediate simulation P_0 was chosen as 0.1.

[Table 2. Summary of all cases in the numerical case studies]

4.1 Identifying the number of delaminations

The numbers of delaminations were identified using the proposed Bayesian approach described in Section 2. The results of the Cases N1 - N5 are summarised in Table 3. From Equation (1), it shows that the probability of a model class M_j is proportional to the evidence value, which can be evaluated using Equation (17) when $O > O_{\min}$.

In order to determine the $O_{\min}$, the value of $V(O)$ is investigated. Figure 5 is used as an example to illustrate the determination of $O_{\min,M_3}$ and the log-evidence for model class M_3 in Case N5. In the figure, $O_{\min,M_3}$ is the value that needs to be determined for model class M_3. Firstly, after the rearrangement of *Y*, the value of $V(O)$ is calculated at each stage. If $V(O)$ reaches its maximal value at this stage, the ranking of the sample corresponding to this maximal $V(O)$ in the ordered list is taken. If this ranking is higher than the ranking $(1-P_0)N$-th (i.e., 450-th for N = 500 and P_0 = 0.1), the Subset simulation proceeds to the next stage. As shown in Figure 5, at stage $_s$ =13 the recorded ranking corresponding to the maximal value of $V(O)$ is 77-th, which is indicated by the vertical dotted line. As this recorded ranking (i.e. 77-th) is higher than 450-th, the Subset simulation stops at this stage, and the value of O corresponding to the 77-th sample is chosen as the $O_{\min,M_3}$, i.e. $O_s > O_{\min,M_3}$ where O_s is the value corresponding to the 450-th sample. Finally, the log-evidence can be obtained using Equation (17). Using the similar approach the estimation of the model log-evidence for all the model classes in Case N5 is shown in Figure 6. The values needs to determined for model class M_1, M_2 and M_3 are $O_{\min,M_1}$, $O_{\min,M_2}$ and $O_{\min,M_3}$, respectively. It is clear from the figure that the model class M_3 has the largest log-evidence value, indicating the most plausible number of delaminations is three for Case N5.

Figure 5. Estimated log-evidence at each stage for model class M_3 in Case N5

Figure 6. Estimated log-evidence of each model class in Case N5

The identification result of the delamination number for Cases N1 to N5 are summarised in Table 3. In the third column, the log-likelihood is taken as the average of

the log-likelihood value of the posterior samples for each model class. In the fourth column, the information gain is calculated as the difference between the model log-likelihood and the log-evidence value illustrating the penalty against the model class with more delaminations. The fifth column is the determined log-evidence of the model class from Equation (15) and the last column is the probability of the model class calculated based on the value of the log-evidence. From Table 3 it is shown that the numbers of delaminations are correctly identified for all cases as the probability of the correct model class is the largest for each case. Specifically, the probability of the model class M_1 with one delamination in Cases N1 to N3 is distinct (e.g., over 98%) from other the model class. While the uncertainty slightly increases in Case N4 as the probability of the model class M_2 with the correct number of delamination is 95.69%. In Case N5, where the actual number of delamination is 3, the probability of the correct identification increases to 99.59%. This is due to the increase of the information gain for the more complex model class, i.e. more delaminations.

[Table 3. Identified number of delaminations in the numerical case studies]

In general, as the number of delamination increases, the log-likelihood indicating the goodness of fitting between the simulation and the measurement also increases. The information gain penalising the complexity of the model class. This provides the log-evidence value for the Bayesian model class selection. Specifically, when the number of delaminations of the corresponding model class is less than the actual situation (e.g., M_1 in Case N4 and M_1 and M_2 in Case N5), the log-likelihood is significantly less than that of other model classes indicating the simulation data is not very well fitted with the measurement data in this situation. On the other hand, when the

number of delaminations (e.g., M_2 in Case N1, M_3 in Case N4 and M_4 in Case N5) is larger than the correct number of delaminations, the log-likelihood increases slightly as the reflected wave from the additional delamination in the SFE model is used to fit the measurement noise and modelling error.

4.2 Identifying the delamination parameters and quantifying the associated uncertainties

In this section the parameters for the delamination are identified for all cases. The influence of the length of delamination on the damage identification is studied in Cases N1 to N3. Cases N1, N2 and N3 considers a delamination with length of 6 mm, 10 mm and 20 mm, respectively, and they are all located at 200 mm from the left beam end. Cases N4 and N5 increase the identification difficulty by considering two and three delaminations with different delamination lengths and though-thickness locations.

The identified results are shown in Table 4. The results of Cases N1 to N5 show that all the delamination parameters are accurately identified. The percentage of error and percentage of sample c.o.v. are also shown in the brackets and squared brackets, respectively. The maximum percentage of error for the identification delamination location and length are 2.34% and 10.09%, respectively. The identified delamination lengths in Cases N1 to N3 show that the error increases with the delamination length. This is because the wave reflection occurs when the incident guided wave entering and leaving the delamination region, and hence, the reflected wave pulse used in the damage identification process is a combination of the two reflected waves. For longer delamination, the reflected wave is usually more complicated. For the identified through-thickness location, although the results of the Delamination 1 in Case N3, and the Delaminations 2 and 3 in Case N5 are one layer different to the true

through-thickness location, the delamination location and length are still very close to the true value. The results show that for cases considered more than one delamination, there is an error in the identified through-thickness location but the delamiatnion location and length can still be accurately identified. In general the sample c.o.v. of the identified delamination length is larger than the delamination location. It should be noted that the amplitude of the reflected wave from the delamination is not a linearly proportional to the delamination size due to the multiple wave reflection when the incident wave entering and leaving the delaminations.

[Table 4. Identified delamination parameters for numerical case studies]

Figure 7. Evolution of the Subset simulation samples for the length of Delaminations 1 and 2 in Case N5

The evolution of the generated samples at each stage in Case N5 using the Subset simulation is shown in Figure 7. The samples converged efficiently to their target distribution from the initial prior distribution, which shows the high efficiency of Subset simulation in generating posterior samples. At Stage 4, the figure show that there are two local optimums and it reduced to a global optimum at Stage 7 and it converged to the final solution at Stage 13. In Figure 8 the marginal PDFs of the delamination length of the Delaminations 1, 2 and 3 in Case N5 were calculated using the adaptive kernel density estimation (Equation (7)) based on the posterior samples generated from Subset simulation. A comparison of the posterior marginal PDFs is shown in Figure 8, the drop in PDF value away from the peak for the Delamination 3 is faster than the Delamination 1 but slower than the Delamination 2. This is consistent to the corresponding sample c.o.v. as shown in Table 4.

Figure 8. Posterior marginal PDFs for the length of Delaminations 1, 2 and 3 in Case N5

5 Experimental case studies

5.1 Experimental setup

Two laminated composite beams with width 6 mm were manufactured from eight HexPly®M21/IM7 unidirectional carbon/epoxy pre-preg with a stacking sequence of $[0/90/0/90]_s$. The pre-preg lamina has a fibre volume fraction of 0.592 and the density is 1.58 g/cm^3. The thickness of each lamina is 0.184 mm. The initial values of the elastic properties were obtained from the material data sheet and calculated using micro-mechanics theory with the consideration of the constituents. The elastic properties were then adjusted such that the discrepancy between the simulated and experimentally measured incident guided wave pulse in the laminated composite beams is minimised. The elastic properties of the lamina are given in Table 5. One of the laminated composite beams has a delamination and the other has two delaminations, and they are named as Cases E1 and E2, respectively. Table 6 summarises the numbers, locations, lengths and through-thickness locations of the delaminations in Cases E1 and E2. The delaminations were generated by inserting thin release films between two laminae at the appropriate though-thickness locations.

[Table 5. Elastic properties of the M21/IM7 pre-preg lamina]

[Table 6. Summary of experimental case studies]

A schematic diagram of the experimental setup is shown in Figure 9. Both sides of the laminated composite beams were fixed at two rigid clamping systems. The length of

the laminated composite beams between the fixed supports is 300 mm. A 6×6×2 mm^3 piezoceramic transducer was bonded to the left end of each of the laminated composite beam. A 6×6×4 mm^3 brass mass was used as the backing mass to enhance the excitability of the A_0 guided wave. The excitation signal was a 50 kHz narrow-band five-cycle sinusoidal tone burst pulse modulated by a Hanning window. The signal was synthetised by a computer and generated by a junction box with the output voltage of 10V. It was then amplified by SERVO-AMP signal amplifier to 50V and applied to the piezoceramic transducer. The out-of-plane displacement of the guided wave signal was recorded using a 1D laser scanning Doppler vibrometer (Polytec PSV-400) with laser controller (OFV5000). The measurement position was located at 60 mm from the left beam end. Signal averaging and band-pass filter were used to further reduce the noise in the measured data. The measured data was then processed by a data acquisition unit and then transmitted back to the computer.

[Figure 9. Schematic diagram of the experimental setup]

5.2 Results and discussions

The identified numbers of delaminations for the experimental case studies are summarised in Table 7. The model class M_1 (single delamination) is selected for Case E1 while the M_2 (two delaminations) is selected for Case E2 based on the calculated probability of the model classes. The results show that the proposed Bayesian approach is able to accurately determine the number of delaminations experimentally. Figure 10 plots the estimate of the log-evidence, i.e., $V(O)$ versus O for Case E2, in which the log-evidence was computed using Equation (17). The identified delamination parameters and the corresponding sample c.o.v.s are shown in Table 8. It is shown that

for Case E1 the delamination location and length are accurately identified and the corresponding percentages of error are 0.10% and 1.57%, respectively. In addition the through-thickness location of the delamination is also correctly determined. Table 8 also show that sample c.o.v.s of the delamination location and length, which are 0.018% and 0.361%, respectively.

[Table 7. Identified number of delaminations in the experimental case studies]

Figure 10. Estimated log-evidence of each model class in Case E2

Case E2 considers the laminated composite beam with two delaminations. Table 8 shows the identified delamination locations, lengths and through-thickness locations, and corresponding percentages of error and sample c.o.v.s. Although the identified through-thickness location of the Delamination 1 is one layer different to the true location, the delamination locations and lengths are still accurately identified. The maximum percentages of error are 2.03% and 0.28% for the identified delamination locations and lengths. Similar to the results in the numerical case studies, the sample c.o.v. of the identified delamination length is larger than the identified delamination location.

Figure 11. Evolution of the Subset simulation samples for the length of Delaminations 1 and 2 in Case E2

Figure 11 shows the evaluation of the samples generated by Subset simulation for the length of the delaminations 1 and 2. It is shown that the samples of delamination lengths efficiently converges to two local optimal regions at Stage 4, and finally

converges to the global optimum at Stage 10. The marginal PDF in Figure 12 shows the uncertainties of the identified delamination length for Delaminations 1 and 2 in Case E2. The uncertainties of both delamination lengths indicated by the marginal PDF are consistent with sample c.o.v.s in Table 8. Figure 12 shows that the drop in PDF value away from the peak for the length of Delamination 1 is much faster than that for Delamination 2, which indicates the uncertainty of the identified delamination length of Delamination 1 is smaller than the Delamination 2.

Figure 12. Posterior marginal PDFs for the length of Delaminations 1 and 2 in Case E2

[Table 8. Identified delamination parameters for experimental case studies]

6 Conclusions

A probabilistic approach has been presented for quantitative identification of multiple delaminations in laminated composite beams using guided waves. The proposed method has addressed a practical situation in the damage detection using model-based approaches, i.e. the number of delaminations is not known in advance for guided wave based damage identification. The proposed method employs the Bayesian model class selection method to select the optimal model class, and hence, the number of delaminations can be accurately identified. In addition to the quantitative identification of the delaminations, i.e. identifying the number of delaminations, delamination locations, lengths and through-thickness locations, the proposed probabilistic approach also quantifies the associated uncertainties. This provides valuable information for engineers in making decision on the remedial work. In this study the time-domain SFE developed based on the higher-order theory and Bayesian updating with Subset simulation have been proposed to further improve the computational efficiency of the

multiple delaminations identification. A series of numerical and experimental case studies have been carried out to verify and demonstrate the capability of the proposed probabilistic approach. The number of delaminations has been determined based on the probability of the modal class calculated using Bayesian model class selection method. The delamination parameters and their associated uncertainties have been identified by calculating their sample means and sample c.o.v.s based on the posterior samples obtained in Bayesian updating with Subset simulation. The results have shown that the probabilistic approach is able to identify multiple delaminations using guided wave signal measured at a single measurement point in the laminated composite beam. All the identified delamination parameters were very close to the true values.

Acknowledgements

The work was supported by the Australian Research Council under grant number DE130100261. The support is greatly appreciated.

References

[1] H.S. Toft, K. Branner, P. Berring, J.D. Sørensen, Defect distribution and reliability assessment of wind turbine blades, Engineering Structures, 33 (2011) 171-180.

[2] A.A. Mosavi, D. Dickey, R. Seracino, S. Rizkalla, Identifying damage locations under ambient vibrations utilizing vector autoregressive models and Mahalanobis distances, Mechanical systems and signal processing, 26 (2012) 254-267.

[3] A. Raghavan, C.E.S. Cesnik, Review of Guided-wave Structural Health Monitoring, The Shock and Vibration Digest, 39 (2007) 91-114.

[4] A.J. Croxford, P.D. Wilcox, B.W. Drinkwater, G. Konstantinidis, Strategies for guided-wave structural health monitoring, Proceedings of the Royal Society, 463 (2007) 2961-2981.

[5] X. Sun, F. Li, X. Miao, G. Meng, L. Zhou, Research on propagation of guided waves in thick beam and crack damage identification, Jixie Gongcheng Xuebao/Journal of Mechanical Engineering, 48 (2012) 1-10.

[6] R. Raisutis, R. Kazys, E. Zukauskas, L. Mazeika, A. Vladisauskas, Application of ultrasonic guided waves for non-destructive testing of defective CFRP rods with

multiple delaminations, NDT & E International, 43 (2010) 416-424.
[7] C.T. Ng, A two-stage approach for quantitative damage imaging in metallic plates using Lamb waves, Earthqu. Struct., 8 (2015) 821-841.
[8] G. Yan, A Bayesian approach for damage localization in plate-like structures using Lamb waves, Smart Materials and Structures, 22 (2013) 035012.
[9] C. Ng, On accuracy of analytical modeling of Lamb wave scattering at delaminations in multilayered isotropic plates, International Journal of Structural Stability and Dynamics, 15 (2015) 1540010.
[10] P. Aryan, A. Kotousov, C. Ng, B. Cazzolato, A baseline-free and non-contact method for detection and imaging of structural damage using 3D laser vibrometry, Structural Control and Health Monitoring, (2016) doi: 10.1002/stc.1894.
[11] R. Schulte, C. Fritzen, J. Moll, Spectral element modelling of wave propagation in isotropic and anisotropic shell-structures including different types of damage, IOP Conference Series: Materials Science and Engineering, IOP Publishing, 2010, pp. 012065.
[12] X. Lin, F.G. Yuan, Damage Detection of a Plate Using Migration Technique, Journal of Intelligent Material Systems and Structures, 12 (2001) 469-482.
[13] E.V. Malyarenko, M.K. Hinders, Fan beam and double crosshole Lamb wave tomography for mapping flaws in aging aircraft structures, The Journal of the Acoustical Society of America, 108 (2000) 1631-1639.
[14] L.F. Rose, C.H. Wang, Mindlin plate theory for damage detection: imaging of flexural inhomogeneities, The Journal of the Acoustical Society of America, 127 (2010) 754-763.
[15] C.T. Ng, M. Veidt, N. Rajic, Integrated piezoceramic transducers for imaging damage in composite laminates, Proceedings of SPIE - The International Society for Optical Engineering, 2009.7493.
[16] S.T. Quek, P. Tua, Q. Wang, Detecting anomalies in beams and plate based on the Hilbert–Huang transform of real signals, Smart materials and structures, 12 (2003) 447.
[17] J. Grabowska, M. Palacz, M. Krawczuk, Damage identification by wavelet analysis, Mechanical systems and signal processing, 22 (2008) 1623-1635.
[18] C.T. Ng, M. Veidt, H.F. Lam, Guided Wave Damage Characterisation in Beams Utilising Probabilistic Optimisation, Engineering Structures, 31 (2009) 2842-2850.
[19] C.T. Ng, Bayesian model updating approach for experimental identification of damage in beams using guided waves, Structural Health Monitoring, 13 (2014) 359-373.
[20] A. Pau, F. Vestroni, Wave propagation in one-dimensional waveguides for damage characterization, Journal of Intelligent Material Systems and Structures, 22 (2011) 1869–1877.
[21] H.K. Noureini, N. Khaji, Detection of a through-thickness crack based on elastic

wave scattering in plates part II: Inverse solution, Asian Journal of Civil Engineering, 13 (2012) 431-454.
[22] M. Krawczuk, Application of spectral beam finite element with a crack and iterative search technique for damage detection, Finite Elements in Analysis and Design, 38 (2002) 537-548.
[23] S. He, C.-T. Ng, Guided wave-based identification of multiple cracks in beams using a Bayesian approach, Mechanical Systems and Signal Processing, 84 (2017) 324-345.
[24] A. Nag, D.R. Mahapatra, S. Gopalakrishnan, Identification of delamination in composite beams using spectral estimation and a genetic algorithm, Smart Materials and Structures, 11 (2002) 899.
[25] J.L. Beck, Bayesian system identification based on probability logic, Structural Control and Health Monitoring, 17 (2010) 825-847.
[26] J.L. Beck, K.-V. Yuen, Model selection using response measurements: Bayesian probabilistic approach, Journal of Engineering Mechanics, 130 (2004) 192-203.
[27] L. Mthembu, T. Marwala, M.I. Friswell, S. Adhikari, Model selection in finite element model updating using the Bayesian evidence statistic, Mechanical Systems and Signal Processing, 25 (2011) 2399-2412.
[28] D. Straub, I. Papaioannou, Bayesian updating with structural reliability methods, Journal of Engineering Mechanics, 141 (2014) 04014134.
[29] S.-K. Au, F.A. DiazDelaO, I. Yoshida, Bayesian updating and model class selection with Subset Simulation, arXiv preprint arXiv:1510.06989, (2015).
[30] M. Chiachio, J.L. Beck, J. Chiachio, G. Rus, Approximate Bayesian computation by subset simulation, SIAM Journal on Scientific Computing, 36 (2014) A1339-A1358.
[31] I. Papaioannou, W. Betz, K. Zwirglmaier, D. Straub, MCMC algorithms for subset simulation, Probabilistic Engineering Mechanics, 41 (2015) 89-103.
[32] M. Muto, J.L. Beck, Bayesian updating and model class selection for hysteretic structural models using stochastic simulation, Journal of Vibration and Control, 14 (2008) 7-34.
[33] J.L. Beck, S.-K. Au, Bayesian updating of structural models and reliability using Markov chain Monte Carlo simulation, Journal of Engineering Mechanics, 128 (2002) 380-391.
[34] J. Ching, Y.-C. Chen, Transitional Markov chain Monte Carlo method for Bayesian model updating, model class selection, and model averaging, Journal of engineering mechanics, 133 (2007) 816-832.
[35] K.V. Yuen, L.S. Katafygiotis, Bayesian Modal Updating Using Complete Input and Incomplete Response Noisy Measurement, Journal of Engineering Mechanics, ASCE, 128 (2002) 340-350.
[36] T. Yin, H.F. Lam, H.M. Chow, A Bayesian probabilistic approach for crack

characterization in plate structures, Computer-Aided Civil and Infrastructure Engineering, 25 (2010) 375-386.
[37] H.-F. Lam, J. Yang, Bayesian structural damage detection of steel towers using measured modal parameters, Earthquakes and Structures, 8 (2015) 935-956.
[38] J.M. Nichols, W.A. Link, K.D. Murphy, C.C. Olson, A Bayesian approach to identifying structural nonlinearity using free-decay response: Application to damage detection in composites, Journal of Sound and Vibration, 329 (2010).
[39] S.K. Au, J.L. Beck, A new adaptive importance sampling scheme for reliability calculations, Structural Safety, 21 (1999) 135-158.
[40] H.-F. Lam, J. Yang, S.-K. Au, Bayesian model updating of a coupled-slab system using field test data utilizing an enhanced Markov chain Monte Carlo simulation algorithm, Engineering Structures, 102 (2015) 144-155.
[41] J. Yang, H. Lam, J. Hu, Ambient vibration test, modal identification and structural model updating following Bayesian framework, International Journal of Structural Stability and Dynamics, 15 (2015) 1540024.
[42] M. Rucka, Experimental and numerical studies of guided wave damage detection in bars with structural discontinuities, Archive of Applied Mechanics, 80 (2010) 1371-1390.
[43] P. Kudela, M. Krawczuk, W. Ostachowicz, Wave propagation modelling in 1D structures using spectral finite elements, Journal of Sound and Vibration, 300 (2007) 88-100.
[44] S. He, C.T. Ng, Analysis of mode conversion and scattering of guided waves at cracks in isotropic beams using a time-domain spectral finite element method, Electron. J. Struct. Eng., 14 (2015) 20-32.
[45] P. Kudela, W. Ostachowicz, A multilayer delaminated composite beam and plate elements: reflections of Lamb waves at delamination, Mechanics of Advanced Materials and Structures, 16 (2009) 174-187.
[46] J.R. Vinson, R.L. Sierakowski, The behavior of structures composed of composite materials, Springer Science & Business Media, 2012.
[47] C.-T. Ng, On the selection of advanced signal processing techniques for guided wave damage identification using a statistical approach, Engineering Structures, 67 (2014) 50-60.
[48] C.T. Ng, M. Veidt, L. Rose, C.H. Wang, Analytical and finite element prediction of Lamb wave scattering at delaminations in quasi-isotropic composite laminates, Journal of Sound and Vibration, (2012).
[49] Hibbett, Karlsson, Sorensen, ABAQUS/standard: User's Manual, Hibbitt, Karlsson & Sorensen, 1998.

Table List

Table 1. Elastic properties of the the pre-preg lamina in the numerical case studies

Properties	E_1 (GPa)	E_2 (GPa)	E_3 (GPa)	G_{12} (GPa)	G_{13} (GPa)	G_{23} (GPa)	υ_{12}	υ_{13}	υ_{23}	ρ (kg/m^3)
Value	128.75	8.35	8.35	4.47	4.47	2.9	0.33	0.33	0.44	1517

Table 2. Summary of all cases in the numerical case studies

Case	Number of delaminations	Delamination location (mm)	Delamination length (mm)	Delamination through-thickness location*
N1	1	$l_1 = 200$	$d_1 = 6$	$k_1 = 3$ or 5
N2	1	$l_1 = 200$	$d_1 = 10$	$k_1 = 3$ or 5
N3	1	$l_1 = 200$	$d_1 = 20$	$k_1 = 3$ or 5
N4	2	$l_1 = 200$	$d_1 = 10$	$k_1 = 4$
		$l_2 = 300$	$d_2 = 6$	$k_2 = 3$ or 5
N5	3	$l_1 = 150$	$d_1 = 4$	$k_1 = 2$ or 6
		$l_2 = 250$	$d_2 = 6$	$k_2 = 3$ or 5
		$l_3 = 350$	$d_3 = 10$	$k_3 = 4$

* Due to the symmetric stacking sequence of the laminated composite beam, the delamination at $k_j = 1, 2, 3$ has the same effect for $k_j = 7, 6, 5$, respectively, on the guided wave reflection and transmission

Table 3. Identified number of delaminations in the numerical case studies

Case	Number of delaminations	Log-likelihood	Information gain	Log-evidence	Probability (%)
N1	**1**	**15853.63**	**4.24**	**15849.39**	99.51
	2	15865.10	21.03	15844.07	0.49
N2	**1**	**15892.59**	**6.72**	**15885.87**	**99.67**
	2	15903.37	23.22	15880.15	0.33
N3	**1**	**14962.32**	**3.83**	**14958.49**	**98.22**
	2	14977.15	22.87	14954.48	1.78
N4	1	6516.87	0.33	6516.54	0
	2	**13787.37**	**18.62**	**13768.75**	**95.69**
	3	13799.22	33.57	13765.65	4.35
N5	1	5877.96	13.63	5864.33	0
	2	7587.29	18.65	7568.63	**0**
	3	**14135.66**	**32.28**	**14103.38**	**99.59**
	4	14153.14	55.27	14097.87	0.41

Table 4. Identified delamination parameters for numerical case studies

Case	Location (mm)	Length (mm)	Through-thickness location
	l_j (sample c.o.v. %) [error %]	d_j (sample c.o.v. %) [error %]	k_i
N1	l_1 = 200.65 (0.019) [0.33]	d_1 = 5.89 (0.298) [1.83]	k_1 = 3
N2	l_1 = 199.85 (0.040) [0.08]	d_1 = 10.73 (0.010) [7.28]	k_1 = 3
N3	l_1 = 197.15 (0.101) [1.43]	d_1 = 22.02 (0.221) [10.09]	k_1 = 3
N4	l_1 = 197.06 (0.001) [2.34] l_2 = 299.31 (0.009) [0.96]	d_1 = 9.45 (0.006) [5.56] d_2 = 5.82 (0.112) [3.33]	k_1 = 3 k_2 = 3
N5	l_1 = 149.35 (0.065) [0.43] l_2 = 249.86 (0.048) [0.06] l_3 = 350.15 (0.029) [0.04]	d_1 = 3.81 (1.596) [4.77] d_2 = 10.57 (0.232) [5.70] d_3 = 5.68 (0.853) [5.33]	k_1 = 2 k_2 = 4 k_3 = 3

Table 5. Elastic properties of the M21/IM7 pre-preg lamina

Properties	E_1 (GPa)	E_2 (GPa)	E_3 (GPa)	G_{12} (GPa)	G_{13} (GPa)	G_{23} (GPa)	υ_{12}	υ_{13}	υ_{23}	ρ (kg/m^3)
Value	160	8.50	8.50	4.20	4.20	2.70	0.35	0.35	0.53	1580

Table 6. Summary of experimental case studies

Case	Number of delaminations-	Delamination location (mm)	Delamination length (mm)	Delamination through-thickness location *
E1	1	l_1 = 100±1	d_1 = 6±0.5	k_1= 3 or 5
E2	2	l_1 = 100±1 l_2 = 200±1	d_1 = 10±0.5 d_2 = 6±0.5	k_1= 4 k_2= 3 or 5

* Due to the symmetric stacking sequence of the laminated composite beam, the delamination at k_j = 1, 2, 3 has the same effect for k_j = 7, 6, 5, respectively, on the guided wave reflection and transmission

Table 7. Identified number of delaminations in the experimental case studies

Case	Number of delaminations	Log-likelihood	Information gain	Log-evidence	Probability (%)
E1	**1**	**9387.94**	**29.84**	**9358.10**	**99.99**
	2	9408.82	60.15	9348.67	0.01
E2	1	6707.91	15.63	6692.28	0
	2	**7342.14**	**24.15**	**7317.99**	**98.39**
	3	7346.68	32.80	7313.88	1.61

Table 8. Identified delamination parameters for experimental case studies]

Case	Location (mm)	Length (mm)	Through-thickness location
	l_j (sample c.o.v. %) [error %]	d_j (sample c.o.v. %) [error %]	k_i
E1	l_1 = 99.90 (0.018) [0.10]	d_1 = 6.09 (0.361) [1.57]	k_1 = 3
E2	l_1 = 100.10 (0.013) [0.10] l_2 = 195.95 (0.011) [2.03]	d_1 = 9.29 (0.147) [7.06] d_2 = 5.98 (0.472) [0.28]	k_1 = 5 k_2 = 3

Figure List

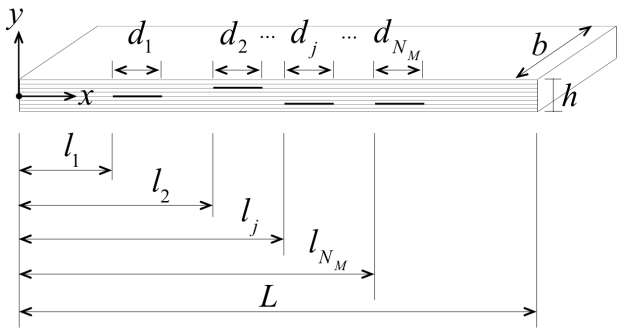

Figure 1. Schematic diagram of the laminated composite beam with multiple delaminations

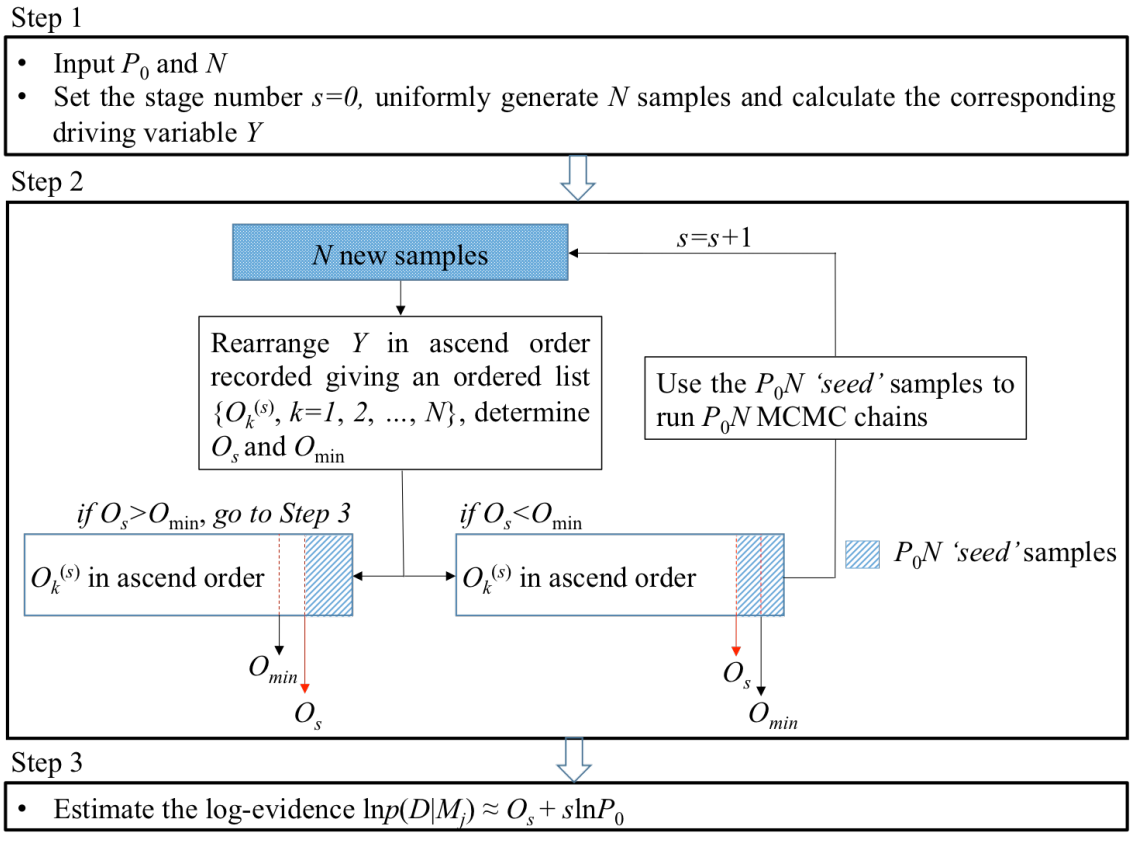

Figure 2. Schematic framework of Subset simulation

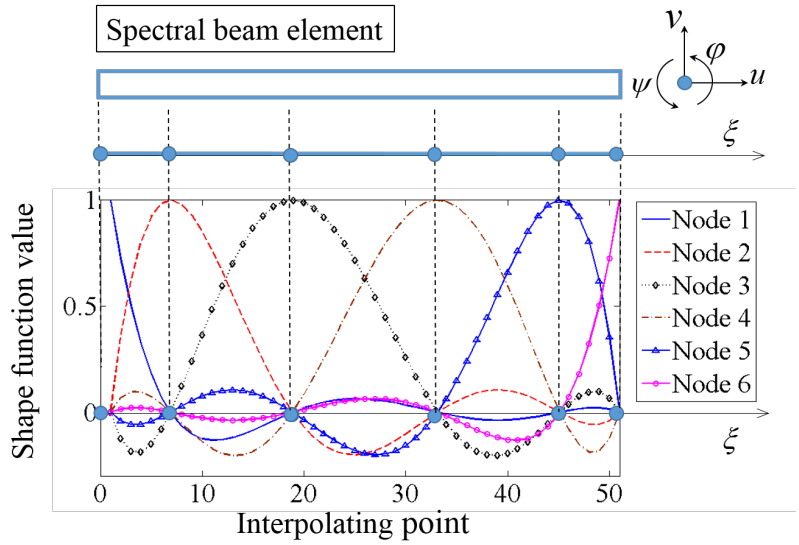

Figure 3. Distribution of the 5th order GLL nodes and the corresponding shape function value of a spectral beam element

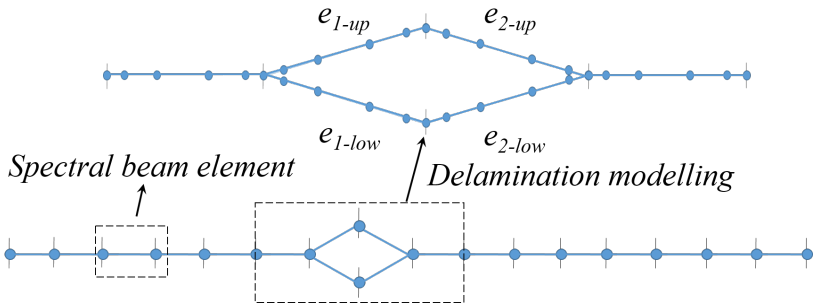

Figure 4. Modelling of laminated composite beam with a delamination and zoom-in at the delamination

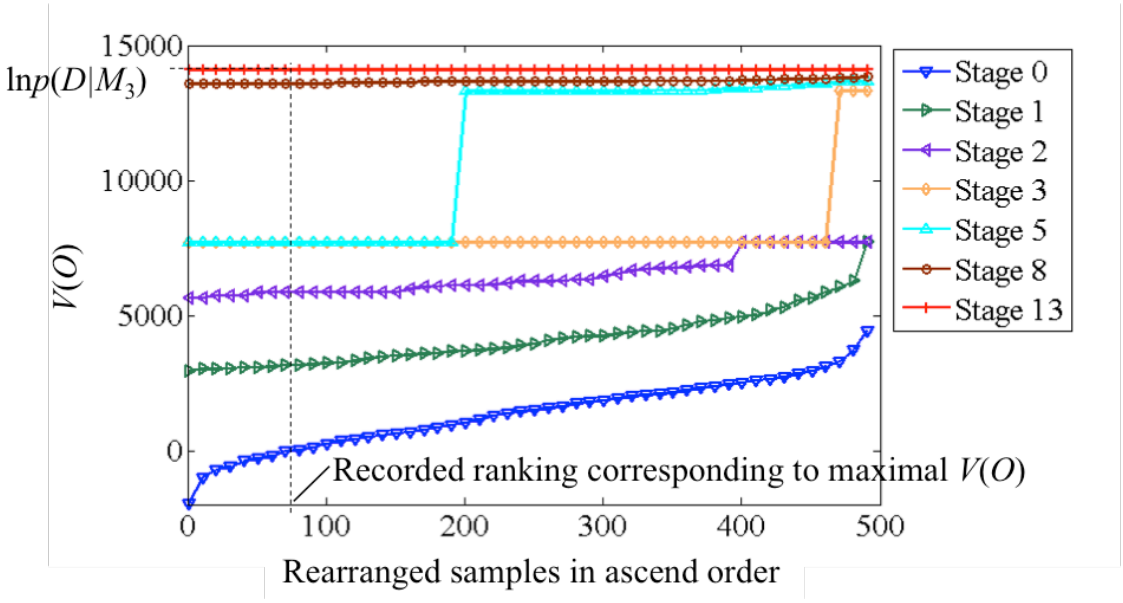

Figure 5. Estimated log-evidence at each stage for model class M_3 in Case N5

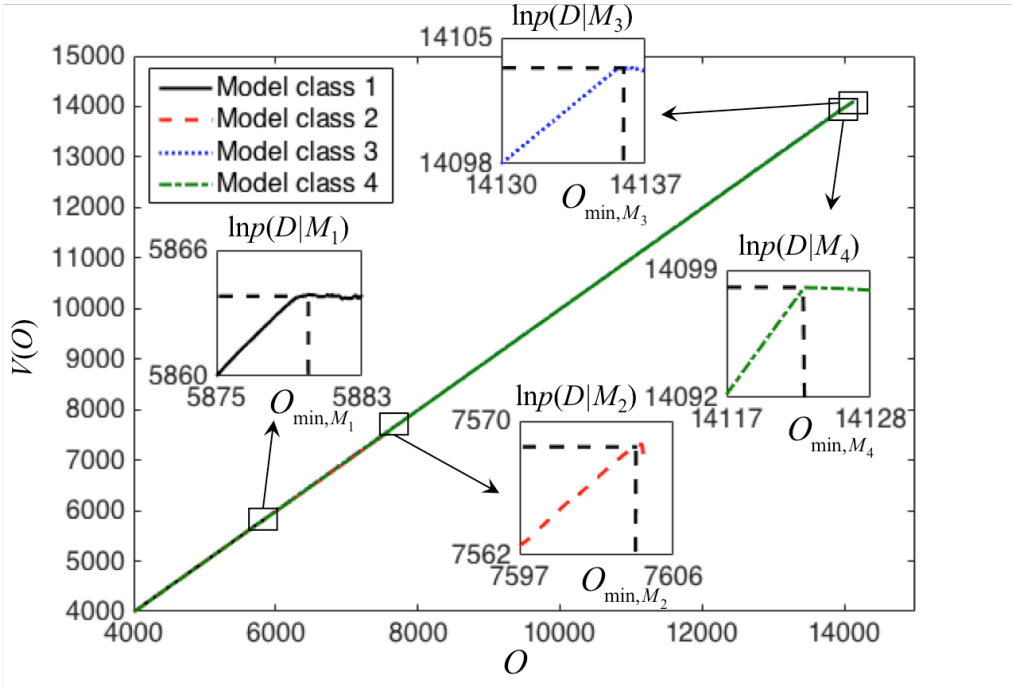

Figure 6. Estimated log-evidence of each model class in Case N5

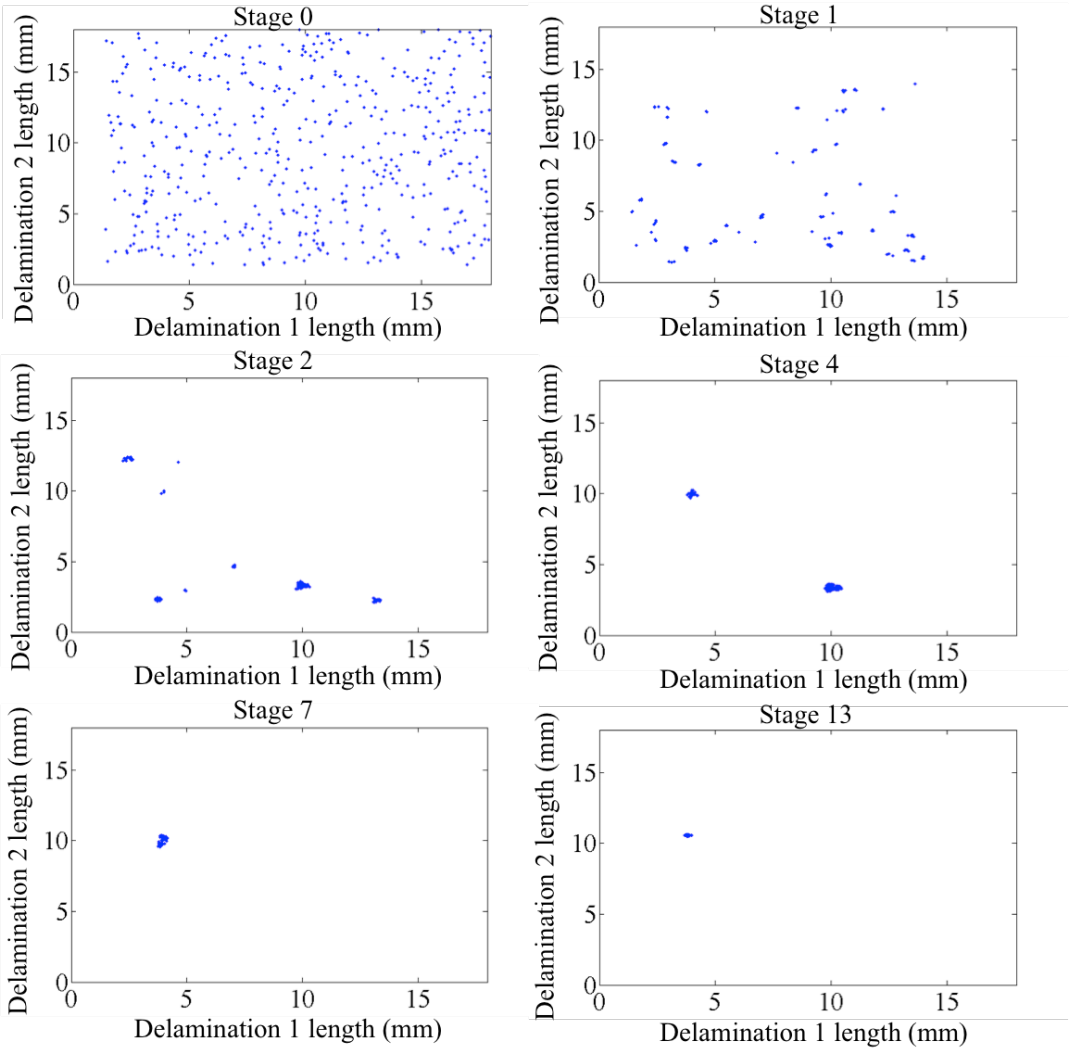

Figure 7. Evolution of the Subset simulation samples for the length of Delaminations 1 and 2 in Case N5

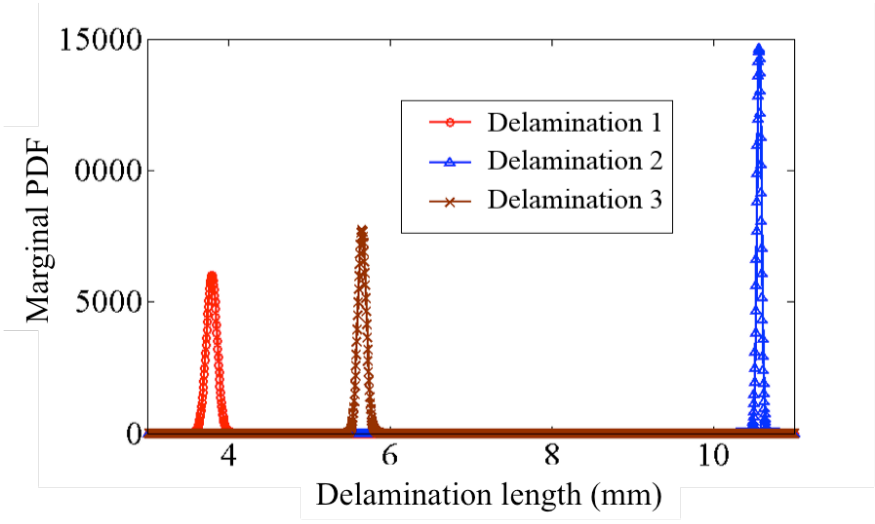

Figure 8. Posterior marginal PDFs for the length of Delaminations 1, 2 and 3 in Case N5

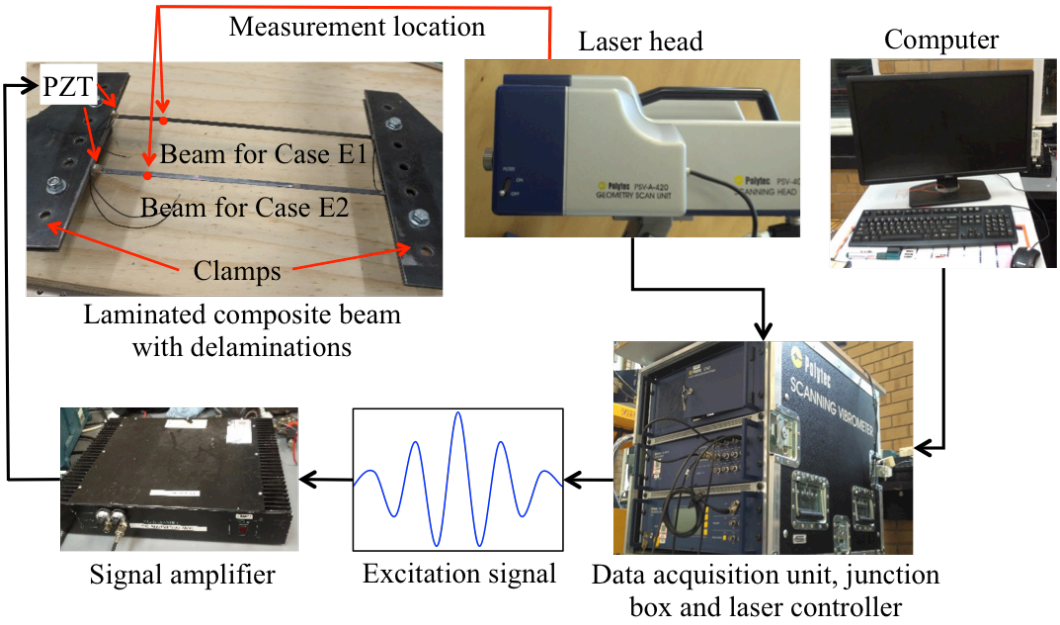

Figure 9. Schematic diagram of the experimental setup

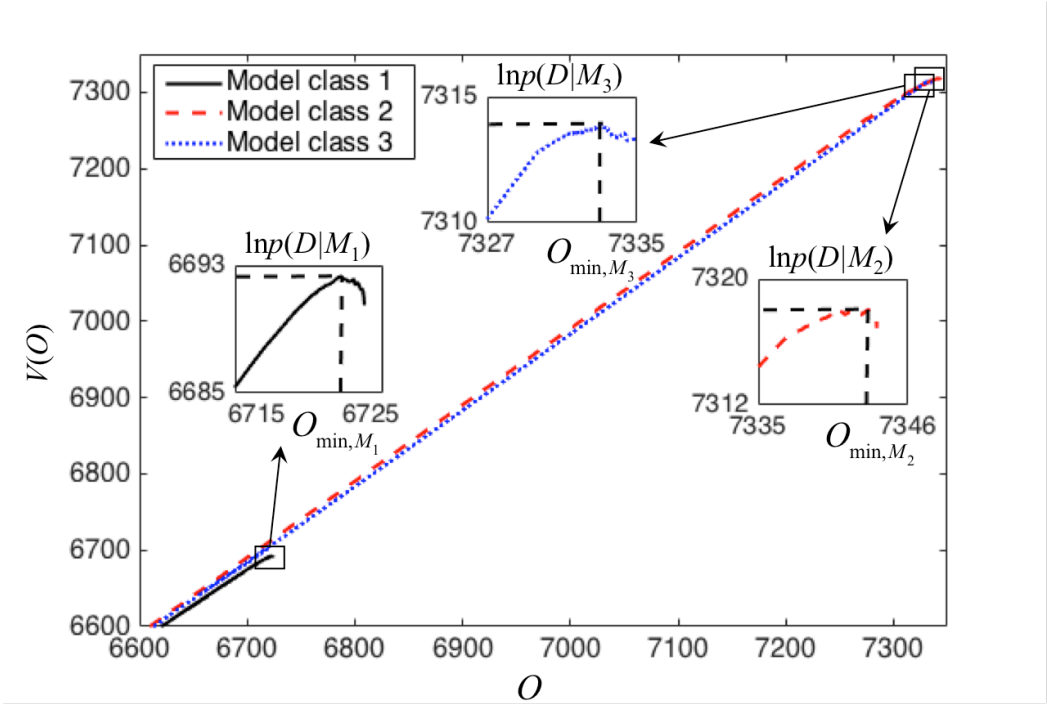

Figure 10. Estimated log-evidence of each model class in Case E2

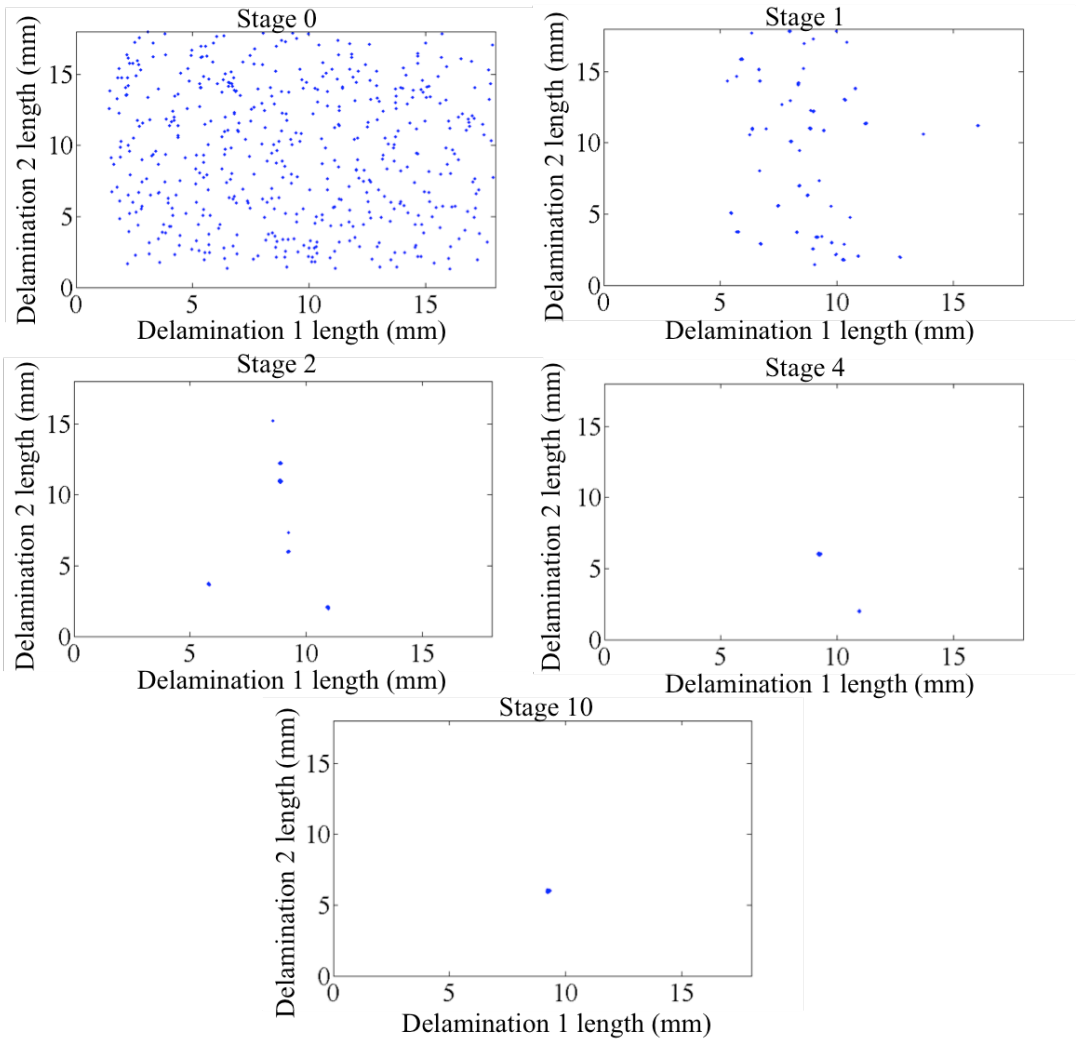

Figure 11. Evolution of the Subset simulation samples for the length of Delaminations 1 and 2 in Case E2

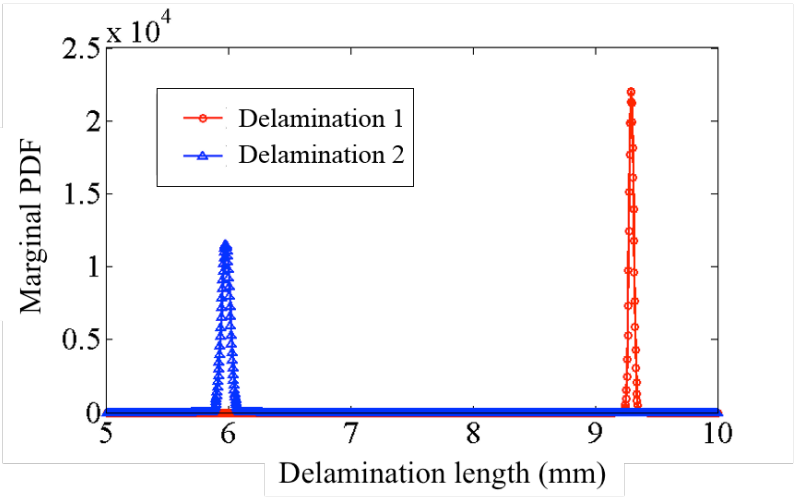

Figure 12. Posterior marginal PDFs for the length of Delaminations 1 and 2 in Case E2